We are IntechOpen,
the world's leading publisher of
Open Access books
Built by scientists, for scientists

4,800
Open access books available

122,000
International authors and editors

135M
Downloads

Our authors are among the

154
Countries delivered to

TOP 1%
most cited scientists

12.2%
Contributors from top 500 universities

CLARIVATE ANALYTICS
BOOK CITATION INDEX
INDEXED

WEB OF SCIENCE™

Selection of our books indexed in the Book Citation Index
in Web of Science™ Core Collection (BKCI)

Interested in publishing with us?
Contact book.department@intechopen.com

Numbers displayed above are based on latest data collected.
For more information visit www.intechopen.com

Estimation of Rotational Axis and Attitude Variation of Satellite by Integrated Image Processing

Hirohisa Kojima
Tokyo Metropolitan University
Japan

1. Introduction

As a result of the increased number of missions in space, the number of satellites that have completed their missions or have broken down has increased, leaving a great deal of space debris in orbit. Most space debris is found in GEO or low-altitude polar orbits and more than 9,600 pieces of debris having a diameter of over 10 cm are currently in orbit. The number of pieces of debris may increase further due to break up, which increases the chance of debris colliding with other spacecraft. To solve this problem, the development of space robots to capture and eliminate space debris from orbit has been explored extensively, and areas such as attitude estimation, formation flying or rendezvous(Kojima , 2005), manipulator control(Inaba & Oda , 2000), de-orbiting of space debris using electro-dynamic tether systems(Forward et al. , 2000; Ishige et al. , 2004) have been investigated. If the target satellite is incorporative, that is, for an example, if radar communication between the target satellite and the debris eliminator satellite is not possible, then image processing will be required in order to monitor the attitude of the satellite and to capture it by means of a robot manipulator. Image processing algorithms with lower computational costs are desired, because the computer resources installed on satellites are usually fewer than those on the ground. A great number of image processing algorithms have been developed for various purposes, such as edge extraction(Harris & Stephens , 1988; Kitchen & Rosenfeld , 1982) and silhouette extraction(Tomasi & Kaneda , 1991). In the EST-VII mission(Inaba & Oda , 2000), the target markers were installed on the daughter satellite so that the mother satellite can easily monitor the attitude of the daughter satellite.

However, normally it is not easy to recognize the attitude of satellites in orbit, because commercial satellites that are not equipped with target markers are usually covered by multi-layer insulator (MLI) with numerous wrinkles that randomly reflect the Sun's light, and such random reflection makes silhouette extraction more difficult. Furthermore, satellites often overlap the Earth, and the direction of the Sun's light relative to the satellite varies with time.

To estimate the attitude of a satellite, the iterative closest point (ICP) algorithm(Besl & McKay , 1992) has been studied by JAXA(Terui et al. , 2002), but this algorithm needs a computational cost. In order to avoid the computational cost of ICP, the grid closest point (GCP) algorithm (Yamany et al. , 1998) was developed using a hash-table technique. The GCP algorithm has

been studied by JAXA and MD-Robotics (Cropp & Palmer , 2002) in Canada. Both ICP and GCP algorithms, however, require a stereovision system to obtain the three-dimensional position of the feature points on the satellite and require a priori reference data in comparing the data set of the feature points on the satellite. Therefore, if a priori reference data is not recorded on the ground in advance, or a stereo camera system is not installed on the debris monitoring satellite, then neither ICP nor GCP can be employed to estimate the attitude of a satellite from the images.

To overcome this problem, the development of an image processing method that can treat wrinkles on the surface of satellites and handle images of satellites overlapping the Earth albedo without using a stereo-vision system is desired. In this paper, such an image-processing scheme is proposed. The proposed scheme consists of six steps: (1) searching the position of a target satellite in the image by color information, (2) extraction of feature points on the satellite using a Harris corner detector (Harris & Stephens , 1988) (3) optical flow estimation by template matching and random sample consensus (RANSAC)(Lacey et al. , 2000), (4) deleting the incorrect optical flow using the epipolar condition(Zhang et al. , 1995), (5) initial guess of the rotational axis and attitude variation from the extracted optical flow by a heuristic approach, and (6)an iterative algorithm to obtain the precise rotational axis and the attitude variation from the initial guess. The image processing method described herein is commonly used for attitude estimation. The contribution of the present paper is the modification of this method by using RGB color information to effectively extract the feature points on a satellite from images, by deleting noises in the images with respect to the consistency of the epipolar condition, and by the heuristic technique to obtain the initial guess of the rotational axis and attitude variation, and shorten the computational cost for the estimation. A space light simulator, which consists of a dark room, is constructed to emulate the light environment in space and is used to verify the validity of the proposed method. The results of experiments using the images of a satellite model taken in the simulation room reveal that the proposed method can estimate the rotational axis and attitude variation of the satellite model under a good lighting condition within approximately 15 deg relative angle, and with an error range of 1.7 deg, which has not yet been achieved under the condition that neither a stereo system nor the priori geometry information of the satellite can be used.

2. In-space lighting simulation room

In order to simulate in-space light conditions, a dark room called the "in-space lighting simulator." was constructed. The dimensions of the in-space light simulator are as follows: height; 2.5 m, width; 2.5 m, and length; 3 m. Figure 1 shows the schematic representation of this simulator which consists of a halogen lamp for imitating the light from the Sun, a reflector for imitating the Earth albedo, and a spacecraft model representing a malfunctioning satellite, specifically, the MDS-1, launched by NASDA. Although the spectral distribution of the halogen lamp is not the same as that of the Sun, the halogen lamp is used in the present study for the sake of simplicity. The albedo of the reflector is set to approximately 0.3 so as to imitate that of the Earth. The reflector is made of high polymeric paper, onto which an image of the Earth, including clouds, is printed. Although MDS-1 was covered with a black multi-layer insulator (MLI), the satellite model in the present study is covered with a gold MLI, because most satellites currently on orbit are covered with gold MLI. The rotational motion of the satellite model is simulated by a three-gimbal system that represents the Euler angles in the form z-y-z, as shown in Fig 2. A commercial digital CCD camera is used to
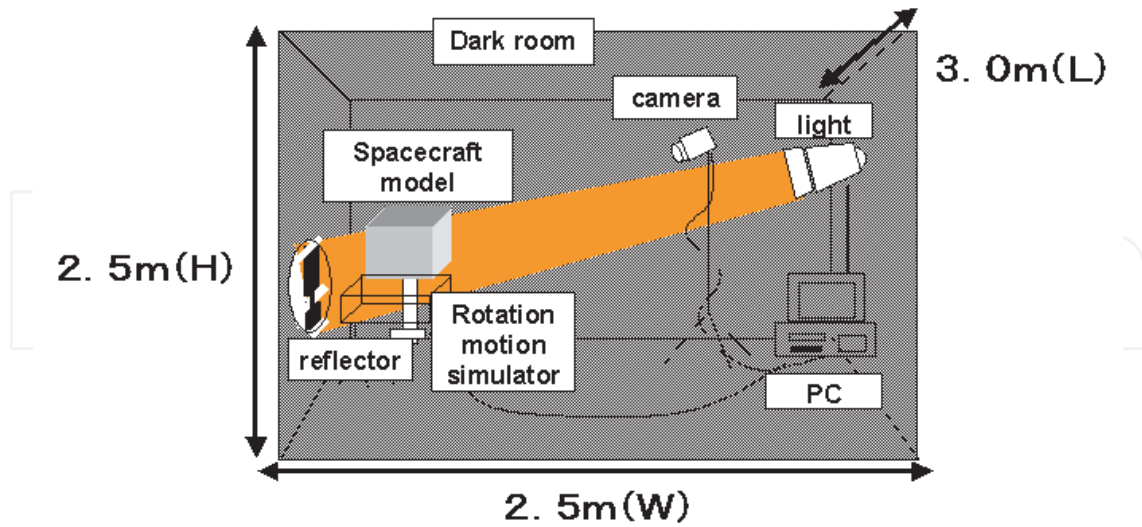
Fig. 1. Schematic representation of the in-space lighting simulator.

Fig. 2. Rotational motion simulator using z-y-z Euler angles.

take images of the satellite model, based on the assumption that such a camera will likely be installed on a debris monitoring satellite in order to reduce the development costs of the satellite.

The sizes of the reflector and the satellite model are determined so as to imitate the relative image, considering the geometric relationship, as shown in Fig. 3, where R is the radius of the Earth, H is the altitude of the satellite with a camera for monitoring debris, and θ is the angle of the Earth as seen from the orbiting satellite with altitude of H. The angle is obtained as a function of R and H as

$$\theta = \arcsin\left(\frac{R}{R+H}\right) \tag{1}$$

Using the distance between the reflector and the digital camera, Z, the diameter of the reflector d is obtained as follows:

$$d = 2Z\tan\theta \tag{2}$$

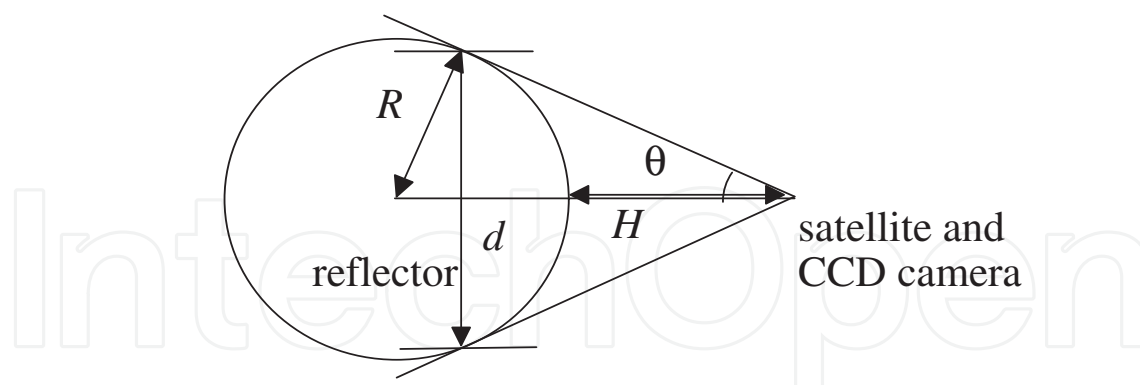Table 1 shows the parameters of the satellite and distance between the satellite model and the

Fig. 3. Geometric relationships between the satellite and the size of the reflector.

Size of Tsubasa	1.2 x 1.2 x 1.5 m
Size of the satellite model	0.21 x 0.21 x 0.21 m
Distance between the satellite model and the reflector	1.5 m
Diameter of the reflector	3.0 m
Emulated altitude	2,500 km

Table 1. Parameters of the In-space lighting simulation.

reflector. The imitated altitude determined from these parameters is also indicated in Table 1. The altitude of the spacecraft in this study is approximately 2,500 km, which is much higher or lower than that of existing debris orbits. The altitude of the satellite model can be imitated by adjusting either the distance between the reflector and the camera, or the distance between the camera and the spacecraft model.

3. Integrated image processing method to estimate attitude variation

The image processing method considered in this study for detecting the rotational axis and attitude variation consists of six steps: (step1) target searching based on color information, (step2) feature points extraction by Harris corner detector(Harris & Stephens , 1988), (step3) optical flow estimation using template matching and random sample consensus (RANSAC)(Lacey et al. , 2000), (step4) deleting incorrect paired points using the epipolar condition(Zhang et al. , 1995), (step5) initial guess of the rotational axis and attitude variation from the extracted optical flow by a heuristic approach, and (step6) an iterative algorithm for obtaining the precise rotational axis and the attitude variation from the initial guess. In this section, each step will be briefly explained.

3.1 Target searching by color information
Before explaining the method used to search the center of the target in the image, the color characteristics of images of a satellite are addressed.
Color images can be typically shown in RGB (red, green, and blue) form. First, single spectra representing these three colors are assumed, respectively, to be:

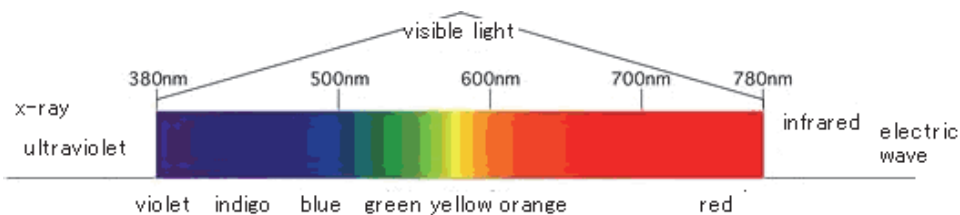$$\bar{r}_\lambda = 700.0[nm], \quad \bar{g}_\lambda = 546.1[nm], \quad \bar{b}_\lambda = 435.8[nm] \tag{3}$$

Fig. 4. Color and wavelength within the rage of the visible light spectrum.

Then, comparing each single spectrum of 1 W with the wave in the range of from 380 nm to 780 nm, which corresponds to the visible wavelength(Fig. 4), yields the distribution of each spectrum. When the color spectrum is given by $C(\lambda)$ W, the RGB value is calculated as

$$R = \int_{380}^{780} C(\lambda)\,\bar{r}_\lambda d\lambda \tag{4}$$

$$G = \int_{380}^{780} C(\lambda)\,\bar{g}_\lambda d\lambda \tag{5}$$

$$B = \int_{380}^{780} C(\lambda)\,\bar{b}_\lambda d\lambda \tag{6}$$

If colors are indicated by eight bits per layer (blue, green, and red), then the number of indicated colors is 16,777,216.

Satellites usually reflect either gold, orange, or yellow, because they are covered by gold multi-layer insulator (MLI), and have solar array panels. On the other hand, the surface of the Earth is blue and white, unless viewed from a high angle. To extract feature points on the satellite efficiently, let us consider the reflection characteristics of the materials of a satellite. Figure 4 shows the relationship between color and wavelength, and Figure 5 shows the distribution of the spectral response of a CCD camera to light of the visible wavelengths. Figures 5(a), 5(b), and 5(c) show the distributions of spectral response of the panel, space, and albedo, respectively, of the upper image. It is found in Fig.5(a) that the RGB brightness of solar array panels has the relation R > G > B.

Taking the above color characteristics into account, the center of the target in the image can be recognized as the center of the areas in which the color distribution is R > G > B as shown in Fig.6. After determining the center of the target, the feature point extraction can be concentrated around the recognized center.

3.2 Extraction of feature points by Harris corner detector

A number of corner detection methods, including Harris(Harris & Stephens , 1988), Kitchen-Rosenfeld, KLT, and SUSAN, have been proposed. A photo image taken in space may include undesired signals for attitude detection due to the effects of camera halation, for example. However, since the Harris corner detector (Harris & Stephens , 1988) is known to be insensitive to noises, in this study, the Harris corner detector is employed to extract the feature points on the satellite model. In this detector, the corner detective function given R_h by
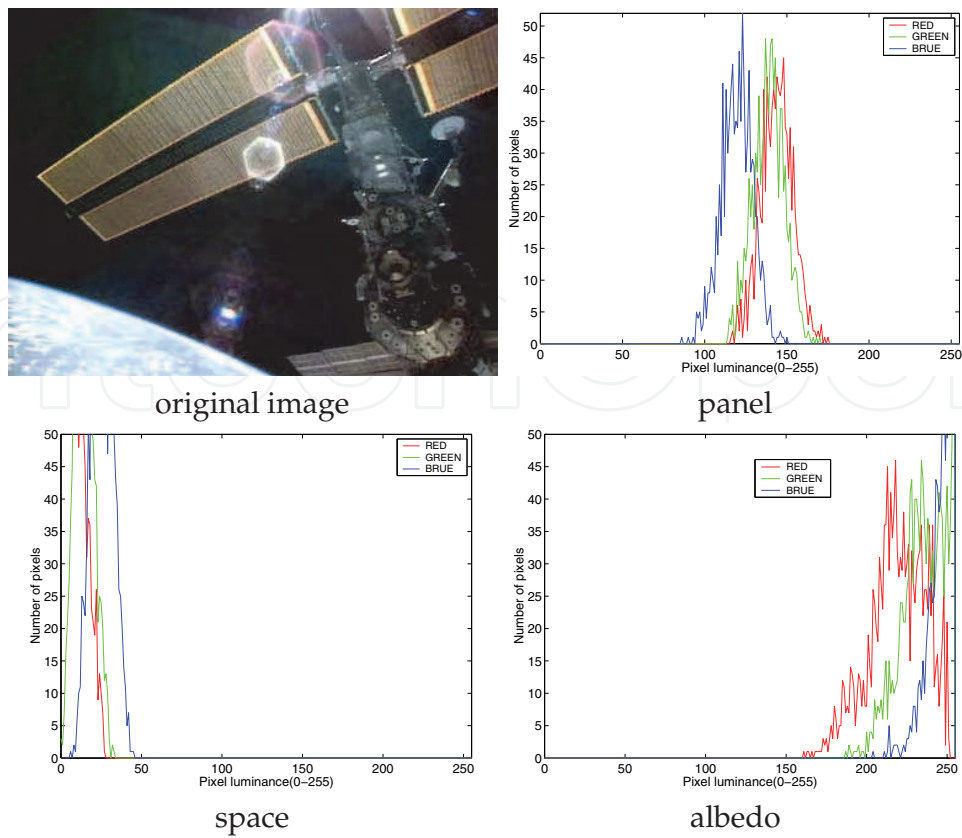
$$R_h = \frac{\det \mathbf{M}}{(tr\mathbf{M})^2} \tag{7}$$

original image

panel

space
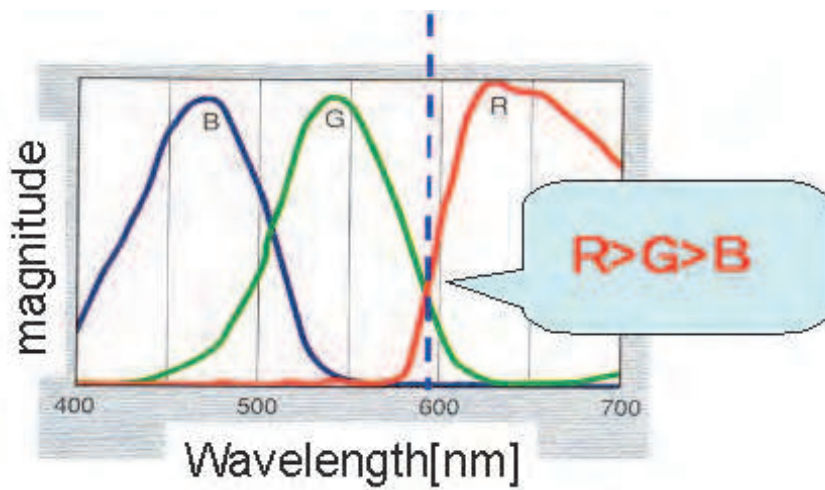
albedo

Fig. 5. Spectral response curve.

Fig. 6. Schematic representation of spectral response curve of the panel.

is used, where the matrix $\mathbf{M}$ is

$$\mathbf{M} = \begin{pmatrix} \left(\frac{\partial I}{\partial j}\right)^2 & \left(\frac{\partial I}{\partial j}\right)\left(\frac{\partial I}{\partial i}\right) \\ \left(\frac{\partial I}{\partial j}\right)\left(\frac{\partial I}{\partial i}\right) & \left(\frac{\partial I}{\partial i}\right)^2 \end{pmatrix} \tag{8}$$

and $I(i, j)$ is the pixel value at an image point (i, j). If the two eigenvalues of $\mathbf{M}$ exceed a specified threshold value, then the corresponding point may be a corner. All of the candidate

corners are checked using the value of R_h, and points with values greater than those of the neighboring points are then extracted as the feature points.

When a color image is directly used in the Harris corner detector, incorrect feature points that are not on the target may be also extracted. In order to eliminate incorrect feature points to the extent possible, the gray scale of the input image was smoothed by an averaged filter, and then candidate feature points were extracted. Feature points were then selected based on RGB color information. As a result of this process, the incorrect were eliminated.

3.3 Paring of the extracted feature points

Two sets of feature points detected by the Harris corner detector are compared, and the points corresponding to the points in the other set are detected by the template matching technique. A template is a pixel data set of size $m \times n$, the center of which is the feature point. The detection process is as follows.

At first, a template of fixed size is generated at each feature point in the first image. The similarity of the template to the feature points in the second image is then calculated. The point with the highest similarity is then accumulated. This process is repeated until all of the candidate corresponding feature points are recorded.

The similarity rate, which is often called the normalized cross correlation function, is given by

$$R_{NCC} = \frac{\sum_{j=0}^{n-1} \sum_{i=0}^{m-1} I(i,j) T(i,j)}{\sqrt{\sum_{j=0}^{n-1} \sum_{i=0}^{m-1} I(i,j)^2 \times \sum_{j=0}^{n-1} \sum_{i=0}^{m-1} T(i,j)^2}} \tag{9}$$

where $m \times n$ is the template size, $T(i,j)$ is the pixel value at the point (i,j) in the template image, and $I(i,j)$ is the pixel value at point (i,j) in the second image.

The correlation range is between 0 and 1. If the value is near 1, then the point has high similarity. Template matching has a limitation with respect to the angle between two groups of the feature points and the rotational velocity of the target satellite. In addition, when the images include the same patterns, the algorithm fails to detect the correct corresponding feature points.

To overcome the above-described template-matching problem, the RANSAC algorithm(Lacey et al. , 2000), which is an optimization method, is used in this study. An initial estimate of the optimal solution is usually required for the optimization methods, but the reasonable selection of an initial estimate is difficult. On the other hand, the RANSAC algorithm does not require an initial estimate because an initial estimate of the solution is randomly set in the algorithm. In addition, the objective function in this method does not need to consider constraints, such as the requirement that certain points be near other points or the requirement that certain points be in the positive range.

In this study, RANSAC is first used to select the candidate corresponding feature points. The template matching method is then employed to detect the optimal correspondence of the feature points.

3.4 Error delete by the epipolar condition

At least eight corresponding points are needed to make an essential matrix that enables detection of the relative translational unit vector, rotational axis vector, and rotational angle of the target. The essential matrix may be not precisely obtained when simply using the

eight-point algorithm (Zhang et al. , 1995) to images of a satellite, because the extracted pairs include incorrect pairs. As such, the following two techniques are employed sequentially to delete probably incorrect paired feature points in this study.

First, an optical flow having a length that exceeds 1.5 times the average of the total optical flow length is deleted because such an optical flow may contain incorrectly paired feature points. Second, an essential matrix is calculated using all of the pairs after deleting the paired points that exceed 1.5 times the average of the optical flow length. If the extracted feature points of images 1 and 2 are represented as $\mathbf{p}_i = [\, u_i \; v_i \; 1 \,]^T$ and $\mathbf{p}_i' = [\, u_i' \; v_i' \; 1 \,]^T$, respectively, then the epipolar condition can be represented as

$$\mathbf{p}_i'^{T}\mathbf{E}\mathbf{p}_i = 0 \tag{10}$$

where $\mathbf{E}$ is the essential matrix. This condition can be converted into a problem to find vector $\mathbf{h}$

$$\min |\mathbf{A}\mathbf{h}| \tag{11}$$

where

$$\mathbf{A} = \begin{bmatrix} u_1 u_1' & u_1 v_1' & u_1 & v_1 u_1' & v_1 v_1' & v_1 & u_1' & 1 \\ u_2 u_2' & u_2 v_2' & u_2 & v_2 u_2' & v_2 v_2' & v_2 & u_2' & 1 \\ \vdots & \vdots & \vdots & \vdots & \vdots & \vdots & \vdots & \vdots \\ u_n u_n' & u_n v_n' & u_n & v_n u_n' & v_n v_n' & v_n & u_n' & 1 \end{bmatrix} \tag{12}$$

$$\mathbf{h} = \begin{bmatrix} h_1 & h_2 & h_3 & h_4 & h_5 & h_6 & h_7 & h_8 & h_9 \end{bmatrix} \tag{13}$$

Using vector $\mathbf{h}$, which is the eigenvector of $\mathbf{A}^T\mathbf{A}$ with the minimum eigenvalues, the essential matrix is given by

$$\mathbf{E} = \sqrt{2} \begin{bmatrix} h_1 & h_2 & h_3 \\ h_4 & h_5 & h_6 \\ h_7 & h_8 & h_9 \end{bmatrix} \tag{14}$$

Each pair of points is confirmed to satisfy the epipolar condition, which is represented by

$$det(\mathbf{E}\mathbf{p}_i) = 0 \tag{15}$$

From the practical point view, it is impossible to satisfy the above epipolar condition. Thus, instead of the above condition, more practical condition is used.

$$det(\mathbf{E}\mathbf{p}_i) \le \epsilon \tag{16}$$

If the epipolar condition is not satisfied within a specified tolerance for a pair of points, then those paired points are deleted to purify the data of the pairs. This verification is repeated several times to obtain a more reliable essential matrix for the paired images.

3.5 Initial guess of rotational axis and attitude variation by a heuristic approach

The final process is the estimation of the rotational axis vector and the attitude variation from the obtained essential matrix. As mentioned earlier, it is difficult to obtain the precise attitude variation using the eight-point algorithm (Zhang et al. , 1995), because the algorithm is originally used on the ground to estimate the motion of the measure camera relative to the static scene. In other words, the motion of the target satellite relative to the chaser satellite's camera is not always equivalent to the motion of the chaser satellite's camera relative to the target without motion. In addition, in a case that the image is taken from the

direction perpendicular to the rotational axis, the optical flow might be likely recognized as the translational motion by the eight-point algorithm.

In order to overcome the above problem, in this study, provided that the translational motion can be cancelled in advance by tracking the center of the target as recognized by means of the color information, and provided that the shape of the target satellite is approximately cylindrical, that is, provided that the optical flow lengths are approximately the same in three dimensions, firstly the following heuristic approach is employed to obtain the initial guess for the rotational axis vector and attitude variation. The iteration based on the least square method is then repeated several time using the initial guess resulting from the heuristic approach to obtain reasonable precision. The objective of the heuristic approach is to reduce the computational cost of the iterative scheme. A schematic diagram of the heuristic approach is shown in Fig.7, and the process is as follows:

(1) Record the maximum length of the optical flow ($F_{\max 1}$) and its direction ($\theta_{\max 1}$).

(2) Rotate the image and the optical flow so that the optical flow with the maximum length follows the y-axis of the camera screen coordinate. Record the length between the center of the target and the y-edge of the target (R_{target}) after rotating the image.

(3) Search the optical flow with maximum x length after rotating the image and the optical flow and recording the optical flow ($F_{\max 2}$).

(4) Determine whether the camera views from the top or bottom of the target by taking the optical flow around the y-edge of the target into account. If the optical flow around the y-edge moves upward, then the camera views the target from the top, otherwise the camera views the target from the bottom.

(5-1) Calculate the inclination of the rotational axis of the target toward the camera view direction, which may be estimated as the ratio between the maximum x length of the optical flow ($F_{\max 1}$) and the maximum y length of the optical flow ($F_{\max 2}$) as follows:

$$v_z = \pm F_{\max 2} / F_{\max 1} \tag{17}$$

The sign of the above equation, plus or minus, is determined in accordance with the direction of the optical flow with maximum x length $F_{\max 2}$ with respect to the y-edge of the target. If the direction is upward and outward, or upward and inward, then the sign is minus. Otherwise the sign is plus.

(5-2) Calculate the inclination of the rotational axis of the target with respect to the y-axis of the camera screen, which may be perpendicular to the optical flow with the maximum length θ_{Fmax1}.

$$v_x = \cos \theta_{F \max 1} \cos \left(\sin^{-1}(v_z) \right) \tag{18}$$

$$v_y = - \sin \theta_{F \max 1} \cos \left(\sin^{-1}(v_z) \right) \tag{19}$$

(6) Calculate the attitude variation (θ_{vary}) from the ratio between the maximum y length of the optical flow ($F_{\max 2}$) and the radius of the target (R_{target}), that is,

$$\theta_{\text{vary}} = \frac{F_{\max 1}}{R_{\text{target}}} \tag{20}$$
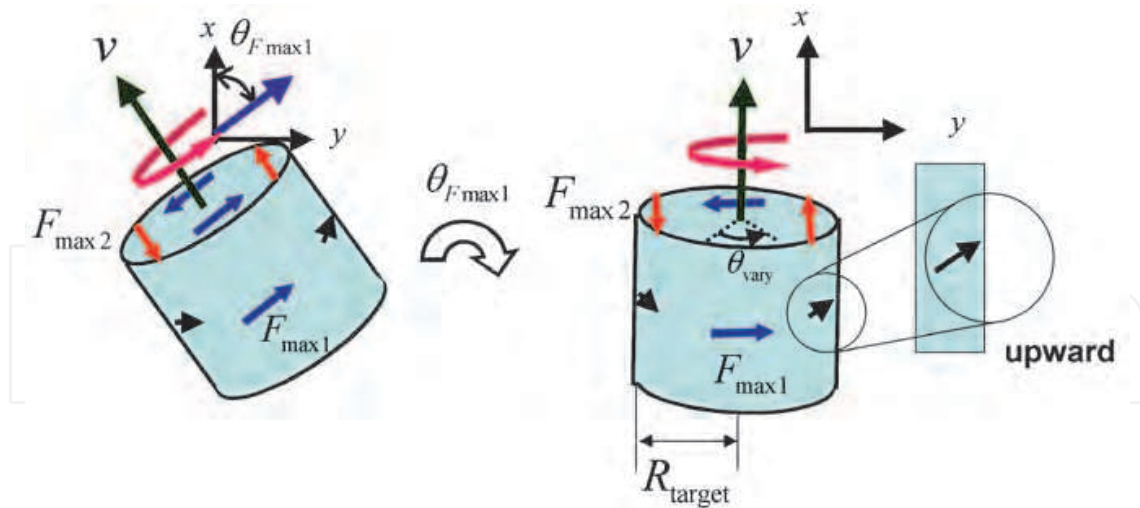
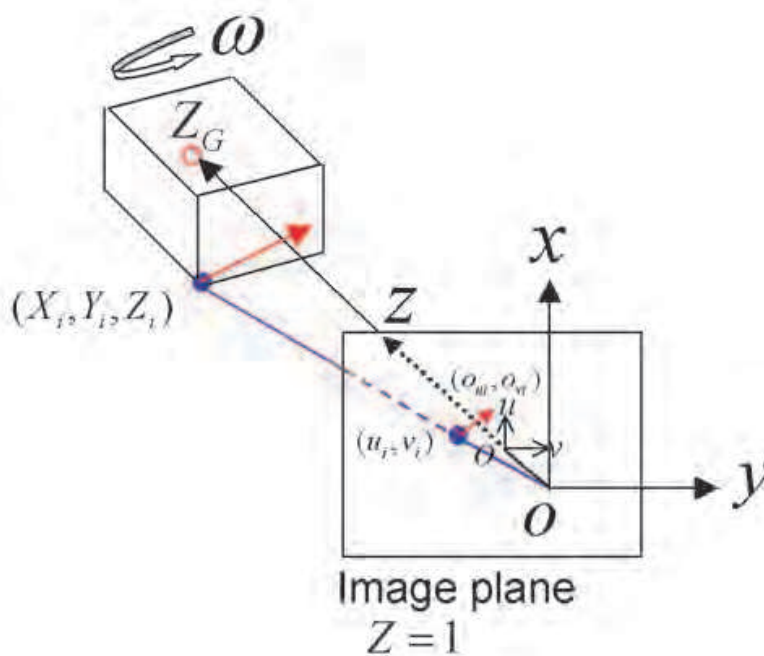Fig. 7. Schematic diagrams for the estimation of the rotational axis.

Fig. 8. Relationships between the rotational motion of the target and optical flow.

3.6 Iterative method for estimating rotational axis and attitude variation, from the initial guess

Figure 8 shows a representation of the relationship between the camera coordinate, the position and optical flow of the feature point. Note that in this study, without loss of generality, the camera screen is assumed to be located at $Z = 1$.

Under the assumption that the translational motion of the target relative to the chaser satellite has been already cancelled by tracking the center of the target image and the center is maintained on the origin of the screen coordinate, each optical flow of the paired feature points

$[o_{ui} \ o_{vi}]^T (= \mathbf{o}_i)$ is represented by

$$\begin{bmatrix} o_{ui} \\ o_{vi} \end{bmatrix} = \left(\begin{bmatrix} 1 & (1+u_i^2) & 0 \\ -(1+v_i^2) & 1 & 0 \end{bmatrix} + \frac{Z_G}{Z_i} \begin{bmatrix} 0 & -1 & 0 \\ 1 & 0 & 0 \end{bmatrix} \right) \begin{bmatrix} \omega_x \\ \omega_y \\ \omega_z \end{bmatrix} \tag{21}$$

where (u_i, v_i) is the position vector of the i-th feature point in the first image, $\boldsymbol{\omega}(= [\omega_x, \omega_y, \omega_z]^T)$ is the rotational angular velocity of the target represented in the camera coordinate, Z_G is the z position of the center of the rotating target, and Z_i is the z position of the i-th feature point in the camera 3D coordinate.
Introducing

$$\mathbf{B}_i = \begin{bmatrix} 1 & (1+u_i^2) & 0 \\ -(1+v_i^2) & 1 & 0 \end{bmatrix} \tag{22}$$

$$\eta_i = \frac{Z_G}{Z_i} \tag{23}$$

$$\mathbf{C} = \begin{bmatrix} 0 & -1 & 0 \\ 1 & 0 & 0 \end{bmatrix} \tag{24}$$

then, Eq.(21) is rewritten as

$$\mathbf{o}_i = (\mathbf{B}_i + \eta_i \mathbf{C}) \, \boldsymbol{\omega} \tag{25}$$

Gathering all the optical flows (21), that is, denoting

$$\mathbf{o} = \begin{bmatrix} \mathbf{o}_1 \\ \mathbf{o}_2 \\ \vdots \\ \mathbf{o}_n \end{bmatrix}, \quad \mathbf{B} = \begin{bmatrix} \mathbf{B}_1 \\ \mathbf{B}_2 \\ \vdots \\ \mathbf{B}_n \end{bmatrix}, \quad \mathbf{C}' = \begin{bmatrix} \eta_1 \mathbf{C} \\ \eta_2 \mathbf{C} \\ \vdots \\ \eta_n \mathbf{C} \end{bmatrix} \tag{26}$$

yields

$$\mathbf{o} = (\mathbf{B} + \mathbf{C}') \, \boldsymbol{\omega} \tag{27}$$

By solving Eqs.(25) and (27) with respect to the relative distance η_i, and the angular velocity of the target ω, one has

$$\eta_i = \mathbf{C}^\# (\mathbf{o}_i - \mathbf{B}_i \omega) \tag{28}$$

$$\omega = (\mathbf{B} + \mathbf{C}')^\# \mathbf{o} \tag{29}$$

where superscript # denotes pseudo inverse matrix.
Starting from the initial guess resulting from the heuristic approach described above, Eqs.(28) and (29) are alternately repeated several times to obtain more precise estimation of the angular velocity (attitude variation) of the target.

4. Experimental results

4.1 Results of searching the center of the target

The Hubble Space Telescope (HST) is chosen as an example of a target. Figure 9(a) shows the input photo image, in which the HST is overlapping the Earth albedo, along with the searched center of the target indicated in green shown in Fig. 9(b). It is seen in Fig. 9(b) that the center of a satellite is almost correctly extracted by the color-information-based method.
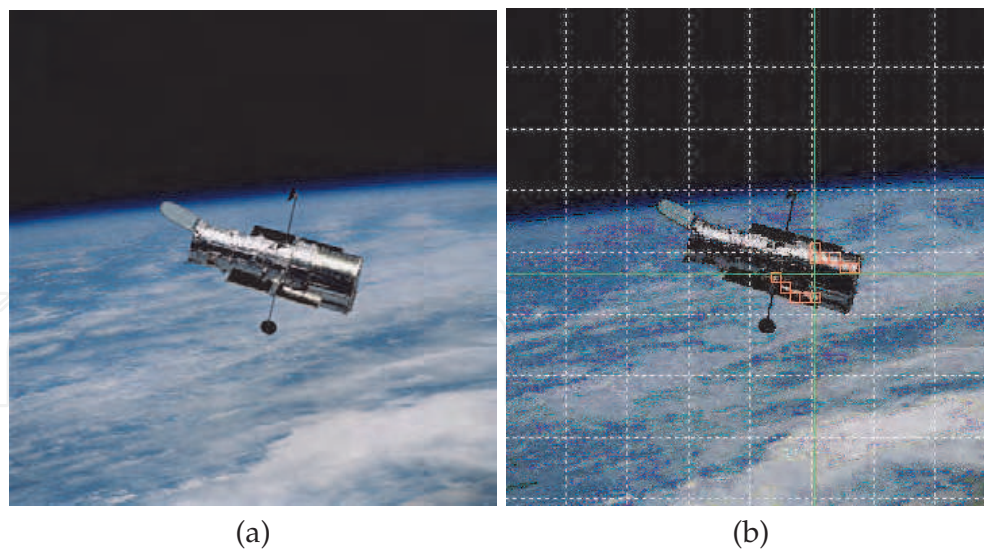
(a)   (b)

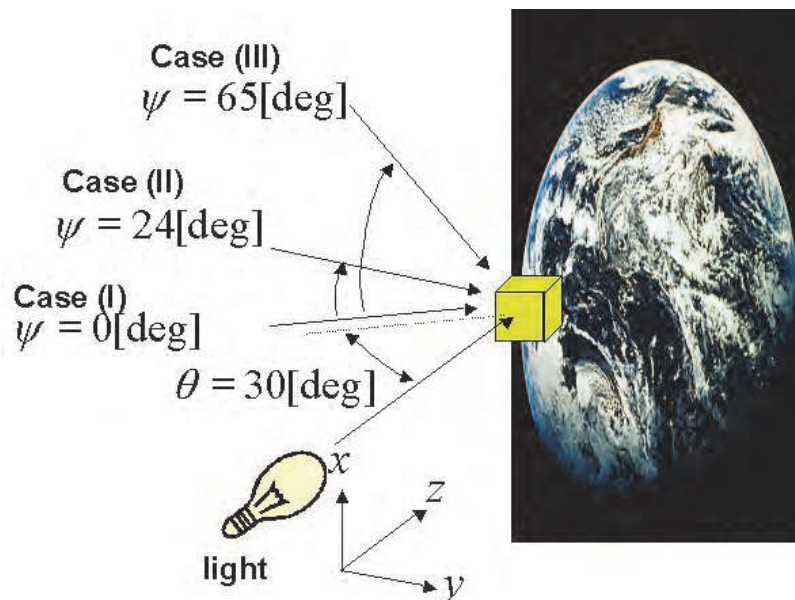Fig. 9. The original image(a) and the detection center of the target.

Fig. 10. Experimental conditions for the CCD camera location

4.2 Results of optical flow detection

A satellite model covered by golden MLI was produced and set on a rotator to emulate rotational motion. For the sake of simplicity, the emulated rotational motion is a single spin at 3 deg/frame around the z-axis. The lighting direction is set to be perpendicular to the reflector. The camera direction with respect to the reflector is set to be inclined at 30 deg. In order to study the effect of the camera view direction on the estimation of the rotational axis and attitude variation, three cases are studied for the camera view direction with respect to the target (as shown in Fig. 10): case (I) parallel to the horizon, case (II) 24 deg from horizontal above the target, and case (III) 65 deg from horizontal above the target.

Two photographs are taken at an angle interval of 3 deg in the in-space lighting simulation room using the rotational motion produced by the rotator. Figure 11 shows the feature points

(a)   (b)
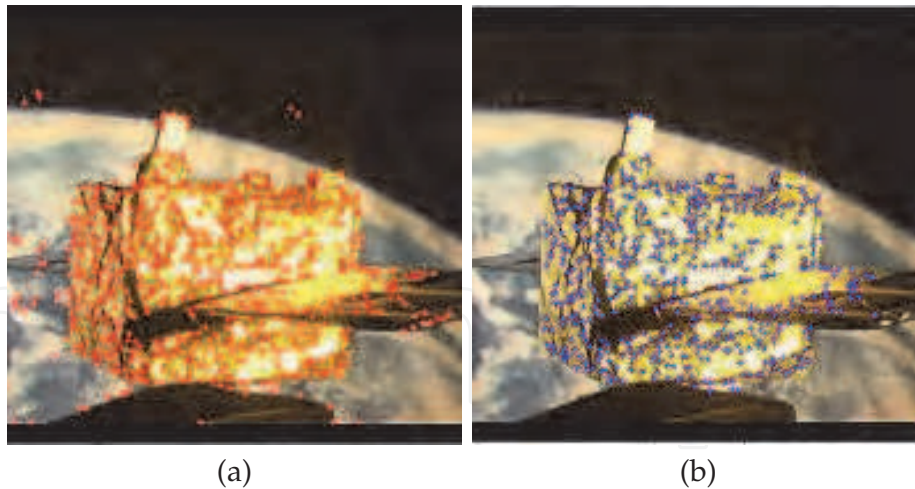
Fig. 11. Feature points extracted by the Harris corner detector without (a) and with employing color information (b).
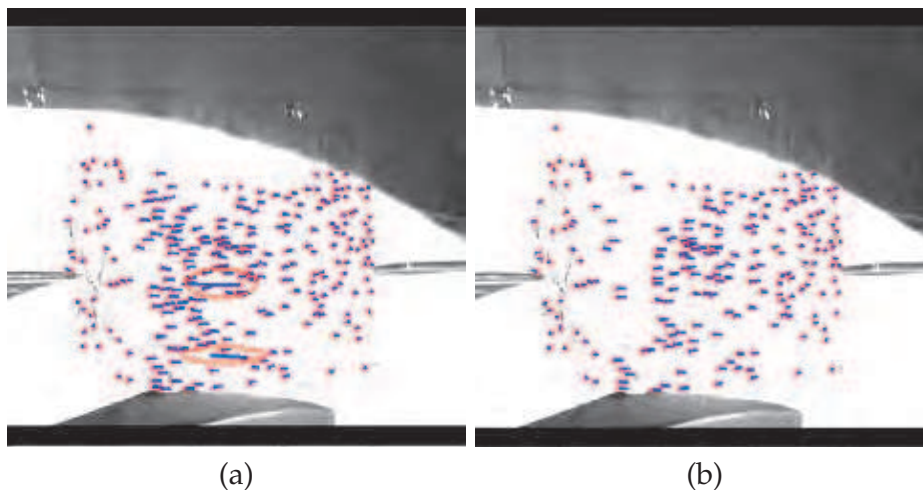

(a)   (b)

Fig. 12. Optical flow extraction before (a) and after (b) eliminating undesired paired points.

extracted by the Harris corner detector, where the threshold for the corner detective function is set to $R_h > 500$.

Figures 12(a) and 12(b) show results of the optical flow before and after deleting the undesired optical flow, respectively. Some undesired flows, which may be caused by incorrectly paired points, are contained in the optical flows, as shown in Fig. 12(a). On the other hand, as shown in Fig. 12(b), all such undesired paired points are successfully deleted, where $\epsilon = 10^{-2}$ is used as the tolerance for epipolar condition. Consequently, the use of the epipolar condition is effective in obtaining the desired optical flow. However, this matching process requires a long time. Thus, a method for reducing the process time of template matching and RANSAC should be investigated to obtain the optical flow within a reasonable process time.

4.3 Results of estimation of rotational axis vector and attitude variation

The results of rotational axis vector and attitude variation estimated by the proposed method according to the frame number are shown in Figs. 13, 14, and 15, respectively, for cases (I), (II), and (III). The correct rotational axis vector and attitude variation are also shown in these figures. The figures show that rough agreement was obtained between the correct direction
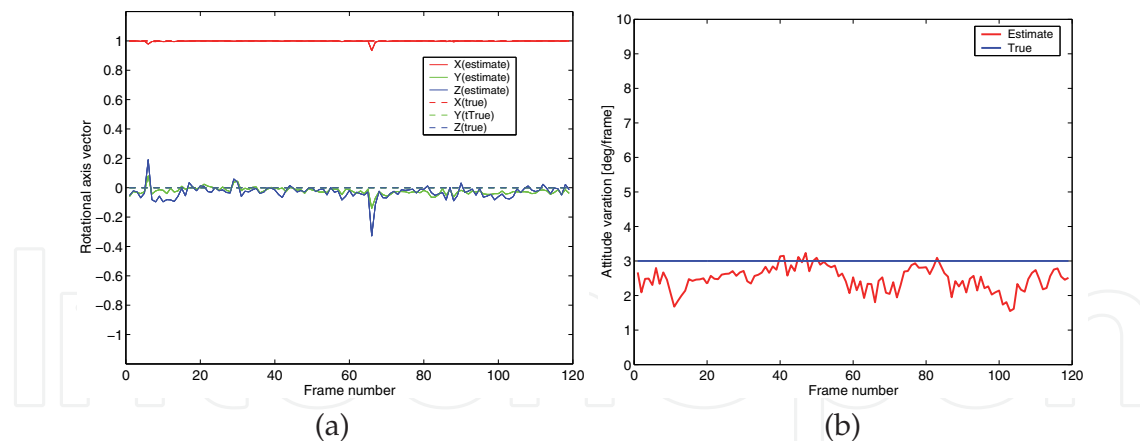
Fig. 13. Estimated rotational axis vector (a) and the attitude variation (b) for case I.
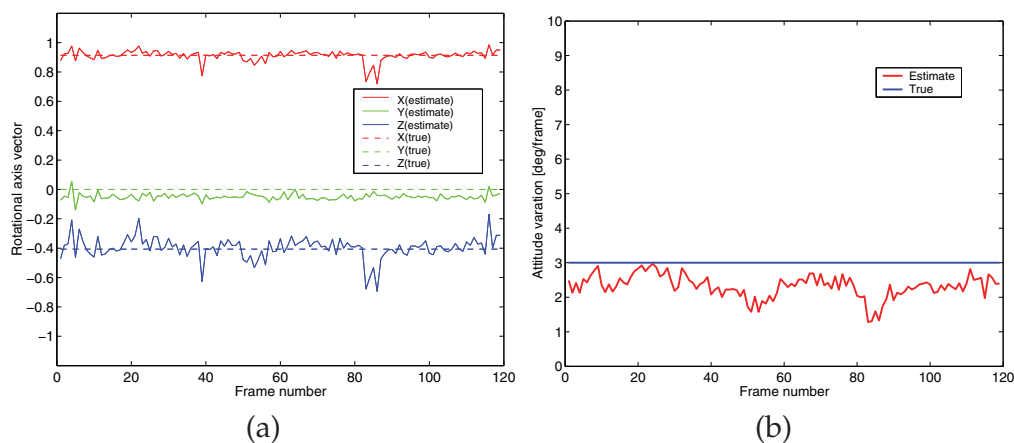

Fig. 14. Estimated rotational axis vector (a) and the attitude variation (b) for case II.
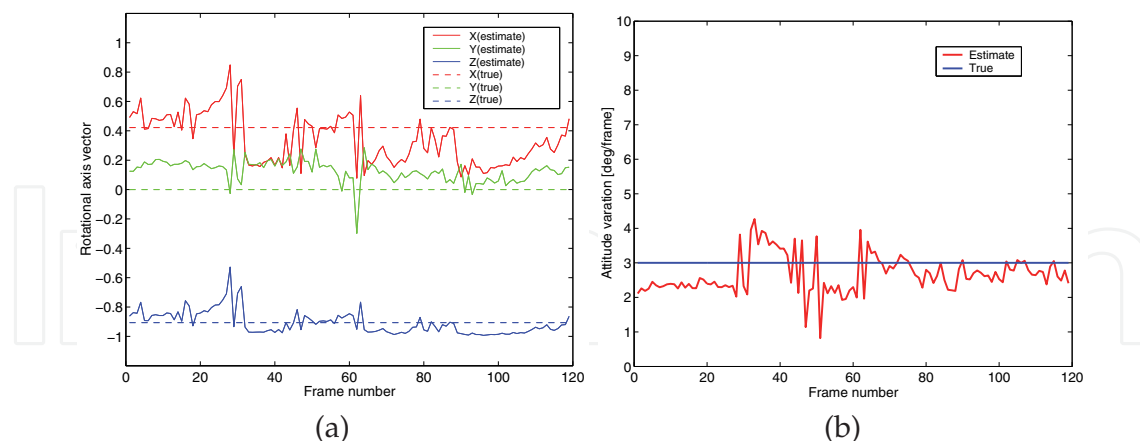

Fig. 15. Estimated rotational axis vector (a) and the attitude variation (b) for case III.

and the estimated direction. The maximum difference between the estimated axis vector and the correct one is approximately 15 deg for cases (I) and (II). The estimated attitude variation per one frame for cases (I) and (II) does not change dramatically, compared to that of case (III), but its mean is less than the correct one by approximately 0.75 deg. This may be because the relative depth ratio, η_i, was estimated to be greater than the correct value due to shade on the target. On the other hand, the estimated attitude variation for case (III) changes dramatically,

compared to that of cases (I) and (II), but the mean of the estimated attitude variation roughly agrees to the correct one. This may be because the reflection of the target was not sufficiently received by the monitoring camera for case (III), in which the mostly observable surface of the target was perpendicular to the light, and this situation resulted in a sensitive estimation to the small number of the extracted optical flow, while the relative depth ratio could be appropriately estimated, compared to cases (I) and (II), because a most observable surface for the camera is a top flat surface of the target, which is almost perpendicular to the camera view direction. The differences of the estimated axis vector and the attitude variation from the correct ones have not yet been achieved under the condition that neither a stereo system nor the priori geometry information of the satellite can be used.

The estimated rotational axis direction oscillates randomly because the MLI wrinkles reflect the light randomly and the heuristic approach described herein estimates the axis based on representative optical flows that depend on random reflections. Furthermore, the estimated attitude variation contains slow oscillations in accordance with the rotational motion of the target. This is because the reflection depends on the angle of the target surface toward the camera view direction and the lighting direction. If taking into account the direction of the reflecting surface to the light direction and the camera view direction, in other words, if the monitoring direction of a camera to the target is appropriately set in order to receive the sufficient reflection, a more precise attitude variation will be obtained. This is a future study.

5. Conclusions

In this study, it was confirmed that feature points and optical flow of a rotating target can be extracted from images taken by only one camera. This was achieved by using the Harris corner detector, template matching, and RANSAC, and by deleting the undesired points in accordance with the RGB color information and the length of the optical flows, even if the optical markers are not equipped on the target. After the optical flow was obtained, the eight-point algorithm was used to obtain a more reliable essential matrix subject to the optical flow. A heuristic approach was introduced to estimate the rotational axis vector and attitude variation by selecting a representative optical flows, provided that the translational motion can be eliminated by tracking the center of the target obtained from the color information. In addition, to improve the rotational axis and attitude variation estimated by the heuristic approach, an iterative square least method was used.

The experimental results showed that the estimated rotational axis vector and attitude variation agree roughly with the correct values under a good lighting condition, but the accuracy is not still yet within an acceptable range for easily approaching or capture in a case that the monitoring direction is approximately perpendicular to the lighting direction, and that they rapidly change due to the random refection of wrinkles of multi-layer insulator. As the next stage, we will attempt to improve the estimation accuracy by taking into account the shade on the target or the lighting direction with respect to the target, and applying some filtering techniques.

6. References

Besl, J. P. & McKay, D. N.(1992). A Method for Registration of 3-D Shapes. *IEEE Transactions on Pattern Analysis and Machine Intelligence*, Vol.14, No.2, (February 1992), pp.(239-256), 0162-8828

Cropp, A. & Palmer, P.(2002). Pose Estimation and Relative Orbit Determination of a Nearby Target Microsatellite using Passive Imagery, 5th Cranfield Space Dynamics Conference, July 2002

Forward, R. L., Hoyt, R. P. & Uphoff, C. W. (2000). Terminator Tether: A Spacecraft Deorbit Device. *Journal of Spacecraft and Rockets*, Vol.37, No.2, (March-April 2000), pp.(187-196), 00224650

Harris, C. & Stephens, M. (1988). A Combined Corner and Edge Detector, *Proceedings of the Fourth Alvey Vision Conference*, Manchester, August-September 1988, pp.(147-151).

Inaba, N. & Oda, M. (2000). Autonomous satellite capture by a space robot world first on-orbit experiment on a Japanese robot satellite ETS-VII, *Proceedings of IEEE International Conference on Robotics and Automation*, San Francisco, April 2000, pp.(1169-1174)

Ishige, Y., Kawamoto, S. & Kibe, S.(2004). Study on Electrodynamic Tether System for Space Debris Removal. *Acta Astronautica*, Vol.55, No.11, (December 2004), pp.(917-929), 00945765

Kitchen, L. & Rosenfeld, A. (1982). Gray Level Corner Detection. *Pattern Recognition Letters*, Vol.1, No.2, (December 1982), pp.(95-102) 01678655

Kojima, H.(2005). Fly-around Motion Control Based on Exact Linearization with Adaptive Law. *Journal of Guidance, Control, and Dynamics*, Vol.28, No.1, (January-February 2005), pp.(167-169) 07315090

Lacey, A. J., Pinitkarn, N. & Thacker, N. A. (2000). An Evaluation of the Performance of RANSAC Algorithms for Stereo Camera Calibration, 11th British Machine Vision Conference, Bristol, September 2000

Terui, F., Kamimura, H., Nishida, S., Takaya, K. & Kawamura, E.(2002). A Stereo Image Processing for the Attitude Estimation of Large Space Debris Objects, *Proceedings of 23rd International Symposium on Space Technology and Science*, Matsue, May-June 2002, pp.(851-856)

Tomasi, C. & Kaneda, T.(1991). Detection and Tracking of Point Features, Carnegie Mellon University, Tech. Report, Pittsburgh, April 1991

Yamany, S. M., Ahmed, M. N., Hemayed, E. E. & Farag, A. A.(1998). Novel Surface Registration using the Grid Closest Point (GCP) Transform, *Proceedings of International Conference Image Processing*, 0-8186-8821-1, Chicago, October 1998, pp.(809-813).

Zhang, Z., Deriche, R., Faugeras, O. & Luong, Q. T. (1995). Robust Technique for Matching Two Uncalibrated Images through the Recovery of the Unknown Epipolar Geometry, *Artificial Intelligence*, Vol.78, Nos.1-2, (October 1995), pp.(87-119) 00043702
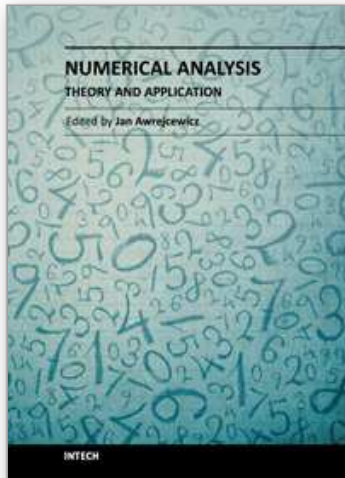
Numerical Analysis - Theory and Application

Edited by Prof. Jan Awrejcewicz

Numerical Analysis â€" Theory and Application is an edited book divided into two parts: Part I devoted to Theory, and Part II dealing with Application. The presented book is focused on introducing theoretical approaches of numerical analysis as well as applications of various numerical methods to either study or solving numerous theoretical and engineering problems. Since a large number of pure theoretical research is proposed as well as a large amount of applications oriented numerical simulation results are given, the book can be useful for both theoretical and applied research aimed on numerical simulations. In addition, in many cases the presented approaches can be applied directly either by theoreticians or engineers.

How to reference

In order to correctly reference this scholarly work, feel free to copy and paste the following:

INTECH
open science | open minds